

Self-Supervised Interactive Object Segmentation Through a Singulation-and-Grasping Approach

Houjian Yu and Changhyun Choi

Department of Electrical and Computer Engineering
University of Minnesota, Twin Cities
{yu000487, cchoi}@umn.edu

Abstract. Instance segmentation with unseen objects is a challenging problem in unstructured environments. To solve this problem, we propose a robot learning approach to actively interact with novel objects and collect each object’s training label for further fine-tuning to improve the segmentation model performance, while avoiding the time-consuming process of manually labeling a dataset. The Singulation-and-Grasping (SaG) policy is trained through end-to-end reinforcement learning. Given a cluttered pile of objects, our approach chooses pushing and grasping motions to break the clutter and conducts object-agnostic grasping for which the SaG policy takes as input the visual observations and imperfect segmentation. We decompose the problem into three subtasks: (1) the object singulation subtask aims to separate the objects from each other, which creates more space that alleviates the difficulty of (2) the collision-free grasping subtask; (3) the mask generation subtask to obtain the self-labeled ground truth masks by using an optical flow-based binary classifier and motion cue post-processing for transfer learning. Our system achieves 70% singulation success rate in simulated cluttered scenes. The interactive segmentation of our system achieves 87.8%, 73.9%, and 69.3% average precision for toy blocks, YCB objects in simulation and real-world novel objects, respectively, which outperforms several baselines. Please refer to our project webpage for more information: <https://z.umn.edu/sag-interactive-segmentation>.

Keywords: Interactive Segmentation, Reinforcement Learning, Robot Manipulation

1 Introduction

Instance segmentation is one of the most informative inputs to visual-based robot manipulation systems. It greatly accelerates the robotic learning process while improve the motion efficiency for target-oriented tasks [13,24,27,40]. However, in real cases, a robot agent frequently encounters unstructured environments and novel objects without a perfect objectness detector trained on corresponding annotations [38,39]. In such a situation, humans often employ multiple interactions with the unknown objects, treating object parts with the same motion pattern

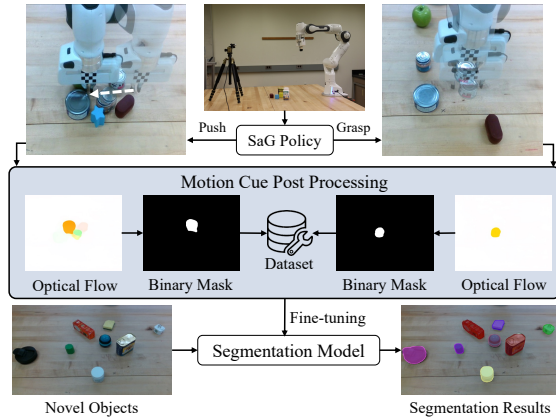


Fig. 1. The robot agent learns a Singulation-and-Grasping (SaG) policy via deep Q-learning in simulation. We collect the RGB images before and after applying the actions and use coherent motion to create pseudo ground truth masks for the segmentation transfer learning.

as a whole. This allows us to eventually get familiar with the objects and understand their shapes and contours [36]. Our work aims to enable robots to perform the same task. Given an imperfect segmentation model and unseen objects, our robot agent learns to obtain object ground truth labels in a self-supervised manner via object pushing and grasping interactions and then recognizes the novel objects.

Classical learning-based segmentation methods, such as ImageNet [33] and MS COCO dataset [28], require a large amount of human-labeled training annotation. While these methods have shown generalization to novel objects to some extent, they underperform when objects are out of the distribution of the trained objects. Interactive segmentation approach has taken an orthogonal avenue by actively collecting labels for novel objects using a robotic manipulator. Pathak et al. uses picking-and-placing [30] and Eitel et al. adopts pushing for singulation [11] to generate single object location displacement and obtain the ground truth label. However, these methods are limited because [30] conducts a simple frame difference method, which is noisy in label annotations and inefficient when multiple objects move simultaneously due to grasping collisions and failures. [11] requires a relatively accurate segmentation method and a large amount of hand-labelled pushing actions to train their push proposal network, [12], in the first place and cannot be directly applied to unseen scenes.

To address the limitations above and obtain high quality object annotations with minimal human intervention, we propose a Singulation-and-Grasping (SaG) self-supervised data collection pipeline free of laborious manual annotation to improve the segmentation results through robot-object interaction. The configuration of Fig. 1 shows our solution. The main contributions of our work are as follows:

- We train the Singulation-and-Grasping (SaG) policy in an end-to-end self-supervised manner via a Deep Q-Network (DQN) without human annotations.
- We propose a data collection pipeline combining both the pushing and grasping motion primitives to generate high-quality pseudo ground truth masks for unseen object. The segmentation results after transfer learning show that our method can be used for unseen complicated shape segmentation in increasingly cluttered scenarios.
- We evaluate our system in a real-world setting without fine-tuning the DQN, which shows the system generalization capability.

2 RELATED WORK

Interactive Segmentation Previous works dealing with the interactive perception problem focus on generating interactions with the environment based on objectness hypotheses and obtaining feedback after applying actions to update the segmentation results in recognition, data collection, and pose estimation tasks [3, 14, 22, 25]. Many methods use a robot manipulator to distinguish one object from others by applying pre-planned non-prehensile actions to specific object hypothesis [6, 26, 35]. However, the non-prehensile action, such as pushing, for a specific object is challenging in cluttered environments due to inevitable collisions with other surrounding objects. Our work utilizes both pushing and grasping actions to facilitate object isolation from a clutter.

The SE3-Net [4] learns to segment distinct objects from raw scene point clouds and predicts an object’s rigid motion, but it only considers up to 3 objects in a less dense clutter. The closest works to our approach are Pathak et al. [30] and Eitel et al. [11] that use grasping and pushing, respectively. However, both of them require collision-free interaction to work effectively. [2] exploits motion cue to differentiate the grasped novel objects from the manipulator and background and gets single object annotation. However, in real cases, the model trained on such data will not reach high performance in heavy clutter. Our Singulation-and-Grasping (SaG) policy manages to solve the collision problem during grasping and even obtains the ground truth annotations during the singulation phase.

Pushing Grasping Collaboration Synergistic behaviors between pushing and grasping have been well explored in [7, 10, 18, 41, 43]. The work in visual pushing for grasping (VPG) [43] provides a model-free deep Q-learning framework to learn joint pushing and grasping policies, where the pushing action is applied to facilitate future grasps. Both [18] and [41] use robust foreground segmentation methods, which track object location through interaction. In such a case, the ground truth transformation for each object can be matched, and the reward based on measurements such as border occupancy ratio [10] can be designed accordingly. [10] and [7] conduct grasps by actively exploring and making rearrangements of the environment until the traditional rule-based grasp detect algorithm, or the DQN decides whether the goal object is suitable for grasping. Analogous to these methods, the visual system in our work cannot provide robust tracking information before and after the interaction. In such a case, the

reward design for our DQN is much harder. The goal of our system is to collect high quality data annotation rather than achieve a simple object removal task.

Object Singulation Previous work [12] effectively solves the singulation problem but uses human-labeled pushing actions to train a push proposal network. [17], on the other hand, selects pushing actions to verify if visible edges correspond to proposed object boundaries without learning features. [34] and [23] focus on the target-oriented object singulation problem, however, it is much more challenging to train a singulation policy that separates all objects than a target-oriented singulation policy that separates only one target object from a clutter. As such, our approach focuses on an object-agnostic singulation problem.

3 Problem Formulation

The interactive object segmentation problem in this paper is formulated as follows:

Definition 1. *Given multiple novel objects on a planar surface, the manipulator executes pushing or grasping motion primitives based on the potentially noisy (e.g. under or over segments) segmentation results. The goal is to improve the segmentation performance via the data collected during robot-object interactions.*

To solve the interactive data collection challenge, we divide the problem into three subtasks:

Subtask 1 *Given an initial unseen cluttered pile of objects, the robot executes objects singulation motions to separate them from each other to create free space for the grasping actions. We define this task as the **singulation** task.*

Subtask 2 *Given a well-singulated scene where the pairwise distance of segments is above a threshold, the robot grasps and removes objects from the scene. We define this task as the **collision-free grasping** task.*

Subtask 3 *Given the RGB images collected from the previous two subtasks, the binary segmentation masks are generated by using learning methods and motion cue post-processing. We define this task as the **mask generation** task.*

4 Method

We model the singulation-and-grasping problem as a discrete Markov Decision Process (MDP) as in [43] and [41]. Given a state s_t , the agent executes an action a_t according to the trained policy $\pi(s_t)$ and obtains the new state s_{t+1} receiving a current reward $R_{a_t}(s_t, s_{t+1})$. The goal of our network is to obtain an action-value function $Q_\pi(s_t, a_t)$ that maximizes the expected reward prediction for each motion primitive. In this section, we also introduce the interactive data collection process, specifically the singulation and collision-free grasping policies, from which we get the objects annotations.

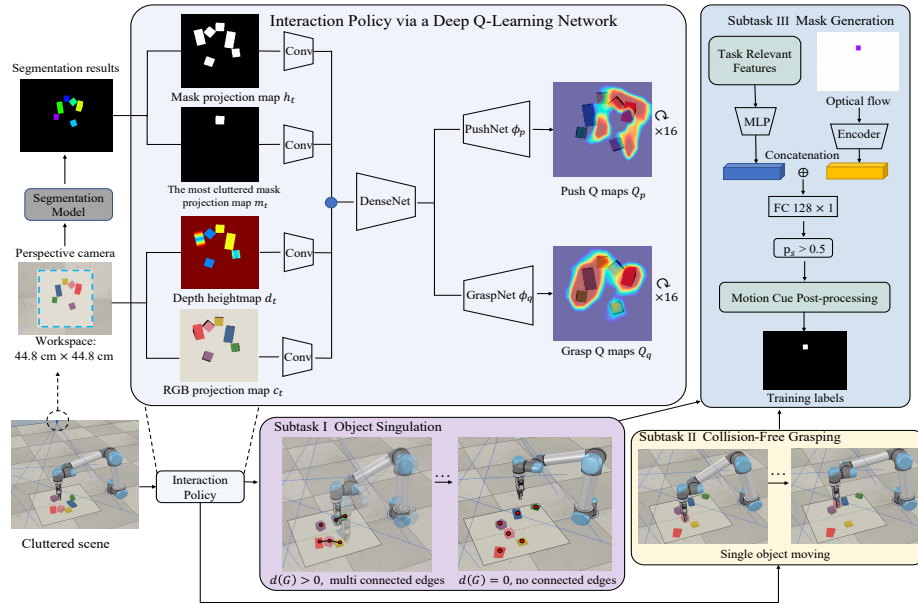


Fig. 2. The interactive data collection pipeline. The deep Q-network takes the state representation s_t as inputs, which consists of the orthographically projected RGB-D images and image segmentation masks. The initially cluttered objects are singulated and grasped via the well trained interaction policy. Both the interaction scenes and the task-relevant features are recorded, focusing on single object moving scenarios to provide accurate object annotations.

4.1 System Model

As illustrated in Fig. 2, a RGB-D camera is affixed to the environment to provide visual information of the workspace. The original RGB-D image I_t at time t is first segmented by a non-finetuned segmentation model to provide objectness hypotheses. Here, we use the UOIS segmentation model [39] taking the RGB and depth images to make inferences. By treating each segmented connected component $\{s^1, s^2, \dots, s^n\}$ as a single object instance, we relabel the segmentation results and get instance center location 2D coordinates $\{c^1, c^2, \dots, c^m\}$ based on their axis-aligned bounding box coordinates.

We orthographically project the RGB, depth, segmentation hypotheses, and the most cluttered mask in the gravity direction with known camera parameters to get the color projection map $c_t \in \mathbb{R}^{H \times W \times 3}$, depth heightmap $d_t \in \mathbb{R}^{H \times W \times 1}$, segmentation projection map $h_t \in \mathbb{R}^{H \times W \times 1}$ and the most cluttered mask projection map $m_t \in \mathbb{R}^{H \times W \times 1}$. The segmentation projection map h_t introduces the global clutter distribution information to the system, while the most cluttered mask projection map m_t highlights the possible target object that requires most effort to be singulated. This additional input m_t intuitively suggests removing the most cluttered area during singulation. While in the grasping stage, m_t is set

to an all-ones map. The state is represented by $s_t = (c_t, d_t, h_t, m_t) \in \mathbb{R}^{H \times W \times 6k}$, where we rotate the state representation k times before feeding in the network. To simplify the motion primitive’s orientation, we set $k = 16$ with a fixed step size of 22.5° w.r.t the z-axis. The feature extractor (a two-layer residual network block [16]) takes s_t as input and further pass to a pre-trained DenseNet-121 [19]. The push net ϕ_p and grasp net ϕ_g finally predict the Q-maps with pixel-wise motion primitive scores. The pushing and grasping motion primitives are executed at the pixel location with the highest Q-value. This network structure is proved to be effective in [43] and [41].

4.2 Singulation-and-Grasping Pipeline

We use the singulation and collision-free grasping motion primitives as the main interaction mechanism. The singulation policy and grasping policy are trained in a multi-stage manner:

Stage I: Singulation Only Training. In this stage, we train a singulation push net ϕ_p for object separation. We initially form a densely-cluttered scene where objects are close to each other. During the singulation stage, an undirected-graph structure $G = (V, E)$ is formed for each state s_t , where $V := \{1, \dots, m\}$, $E \subset V \times V$ and each node $i \in V$ is represented by c^i . The edge E is constructed by the pairwise node Euclidean distance. When the pairwise distance is under some constant threshold p , we claim that the edge of the two nodes is connected. We then find the most cluttered mask from the segmentation hypothesis that corresponds to the largest number of connected edges.

The perception model then provides under-and-over segmentation as a zero-shot inference. We obtain the graph density value as indicated in [8]

$$d(G) = \frac{2|E|}{|V|(|V| - 1)} \quad (1)$$

where $|E|$ represents the number of the edges and $|V|$ is the number of the vertices. For a cluttered scene, the vertices in the graph are highly connected and the density value $d(G)$ is close to one. In contrast, when objects are well singulated, the density value $d(G)$ is around zero.

Existing target-oriented methods have a strong assumption that a target object can be robustly detected [40, 41]. In contrast, our segmentation model cannot track the pushed objects, which makes designing the reward more difficult. A good pushing motion is supposed to create an end-effector trajectory across the segmentation masks but also separate the under-segmented clutter resulting in a non-decreasing of total mask numbers. Moreover, both the increasing average pairwise distance of two objects and the decreasing of graph density $d(G)$ indicate effective pushes. On the other hand, we also fit the center location representation as a two-dimension random variable into a multivariate Gaussian

distribution. The determinant of the covariance matrix indicates the sparsity of the spatial distribution. Therefore, we design the pushing reward function as:

$$R_p = \begin{cases} -0.5, & d(G) \text{ increases} \\ 0.25, & \text{pushing passes mask } h_t \text{ and} \\ & |\{c^1, \dots, c^m\}|_{t+1} \text{ non-decrease} \\ 0.5, & a_d \text{ or } a_{var} \text{ increases} \\ 1.0, & d(G) \text{ decreases or } u \text{ increases} \end{cases} \quad (2)$$

where a_d and a_{var} show the average and variance of the pairwise center location distance, respectively. $|\{c^1, \dots, c^m\}|_{t+1}$ indicates the number of instance masks at time $t + 1$. u represents the covariance matrix determinant value.

Stage II: Grasping Only Training. In this stage, the parameters of the pretrained push net ϕ_p are fixed and we mainly train a grasp net with a relatively scattered scene to simulate the scenario where objects have already been well singulated. Similar to [43], we conduct object-agnostic grasping tasks and use the similar reward function here:

$$R_g = \begin{cases} 1.5, & \text{if grasping successfully} \\ 0, & \text{otherwise} \end{cases} \quad (3)$$

Since the previous stage has created enough space for object-agnostic grasping, the rational explanation for training a grasp-only policy is to maximize the grasping success taking advantage of stage I.

Stage III: Coordination. In this stage, we combine the stage I and II as the interaction policy for pushing and grasping collaboration. The pushing action is executed iteratively until the graph density value $d(G)$ reaches zero or the maximum pushing number, while the grasping action dominates the later process.

Algorithm 1 (see Supplementary Section 1) summarizes the details of the interaction policy. Our SaG interactive policy training and implementation details can be found at Supplementary Section 2.

4.3 Mask Generation

Prior work [11] has explored the similar idea, but it cannot filter out multi-object moving scenarios which generates false positive training labels that negatively affects the transfer learning.

Therefore, we propose a optical flow learning-based binary classifier to identify single object moving cases and apply the motion cue post-processing method on them. The implementation details will be discussed in Supplementary Section 2. The classifier takes optical flow and task relevant features as input and outputs the single object moving probability. Since that the training data for our flow classifier is collected from simulation only, and the real robot setting optical flow computation has a domain gap from simulation, we consider adding such task relevant features from pushing and grasping history to help the flow

classification. The task relevant features consist of graph density $d(G)$, average and variance of pairwise center location distance a_d and a_{var} and target border occupancy ratio r_b (defined in [41]). We obtain object’s ground truth location directly from V-REP and by comparing the object locations change, we set the probability of single object movement to be 1 as the ground truth label when only one object was moving and 0 otherwise.

We compute the optical flow using the FlowNet2 [20] with images I_t and I_{t+1} before and after executing the motion primitive a_t and feed the optical flow together with task relevant features to the classifier. Similar to [11], we use normalized graph cut on each optical flow to obtain a set of segments in binary mask format $L_t = \{l_t^1, \dots, l_t^N\}$ for frame I_t , and we only select segment $l_t^n \in L_t$ that satisfies related constraints (e.g., mask size). We add the RGB image I_t and its corresponding binary mask l_t^n as a ground truth label into the training dataset $D = \{(I_0, l_0^{n_0}), \dots, (I_t, l_t^{n_t})\}$ for fine-tuning.

4.4 Mask R-CNN Transfer Learning

We use the Mask R-CNN [15] pretrained COCO instance segmentation baseline with the ResNet-50-FPN backbone implemented by Detectron2 [37]. It’s a common practice to use a baseline model pretrained on a well-annotated standard image dataset, for instance ImageNet [33], where the backbone serves as a universal feature extractor in the network. Moreover, the Feature Pyramid Network (FPN) type backbone extracts image features from different scales, which provides better anchors prediction in various levels. The details of segmentation results can be found at Section 5.

5 Experiments

In this section, we conducted multiple experiments to evaluate the proposed Singulation-and-Grasping (**SaG**) approach. The goals of the experiments are 1) to compare our **SaG** with several baselines in both singulation and segmentation performances. 2) to show whether the fine-tuned **SaG** segmentation model is effective in other downstream robot manipulation tasks.

5.1 Datasets and Evaluation Metrics

Singulation We evaluate our singulation performance in simulation with 6 basic shape toy blocks. We conduct 200 test trials with various object arrangements for the 6-object singulation task with the proposed approach and record $d(G)$ values. A trial is considered to be successful when all object pairwise distances are above some threshold p and $d(G)$ reaches zero within 8 pushes.

Segmentation We collect 404 and 200 testing images w.r.t toy blocks and YCB [5] objects in simulation. For default test setting, we randomly drop 10 toy blocks and 8 YCB objects in the workspace. Moreover, for cluttered test setting, we increase the object number to 18 toy blocks and 15 YCB objects where all

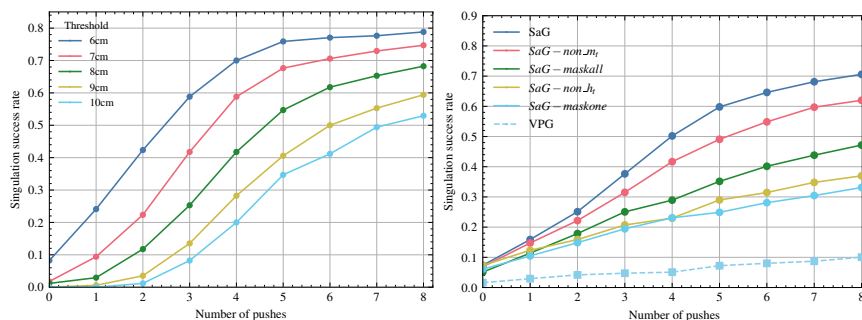


Fig. 3. Singulation policy performance with different distance thresholds. **Fig. 4.** Singulation success rate for different baselines.

objects are located in a dense clutter. For real robot default testing, we manually labeled 100 images with 6 to 8 objects in the workspace. Moreover, 50 images are labeled with up to 16 objects in a clutter for the cluttered test cases.

We evaluate the instance segmentation performance with the standard MS COCO evaluation metric average precision (AP). We also use another evaluation metric as defined in [9] to compare current state-of-the-art non-interactive segmentation method, where scores for segmentation instances are not provided and cannot be evaluated with COCO AP. To compute the overlap precision, recall and F-measure (P/R/F), the Hungarian matching method is used for the predicted and ground truth masks. Given the matching, the P/R/F is computed by $P = \frac{\sum_i |a_i \cap g(a_i)|}{\sum_i |a_i|}$, $R = \frac{\sum_i |a_i \cap g(a_i)|}{\sum_j |g_j|}$, $F = \frac{2PR}{P+R}$, where a_i denotes the set of pixels belonging to predicted object i , $g(a_i)$ is the ground truth matched to each predicted region, and g_j denotes ground truth pixels of object j .

5.2 Singulation Performance

We utilize the same simulation environment in V-REP [32] utilizing a UR5 arm with an RG2 gripper.

Five baselines are compared with our approach: 1) **SaG-maskall**, the baseline without the most cluttered object mask projection map m_t from our system and filters the Q maps by the binary mask projection map h_t . 2) **SaG-maskone**, the baseline without the m_t input and filters the Q maps with m_t . 3) **VPG**, target agnostic pushing and grasping to clean the cluttered objects [43] with no modification. 4) **SaG-non- m_t** , our proposed method without m_t . 5) **SaG-non- h_t** , our proposed method without h_t .

Fig. 3 indicates the average singulation success rate with different pairwise distance thresholds p from 6cm to 10cm versus the number of pushes. The pushing motion primitives achieve about 80% singulation success rate with small threshold of 6cm and over 50% with large threshold of 10cm after eight pushes.

To fairly show that **SaG** is effective, we further conduct the five push-only baseline comparisons mentioned above. We reuse the test cases when evaluating

SaG singulation success for each method. The average singulation success rate for each baseline combines performance measurement with thresholds from $6cm$ to $10cm$. Fig. 4 demonstrates that the **VPG** push-only method barely has the object singulation effect. On the other hand, our proposed approach improves the performance by a large margin about 60% after eight pushes. Although the singulation task is target-agnostic, **SaG-non- m_t** and **SaG-non- h_t** indicate that providing the network with global and local clutter information will help improve the overall performance. **SaG-maskall** in such a case may push objects that have already been well singulated resulting in an ineffective pushing policy. While **SaG-maskone** always pushes the most cluttered mask, it lacks the global clutter state reasoning, which results in unsatisfactory performance.

Table 1. Segmentation results in simulation with toy blocks. Ablation study on different architectures of SaG pipeline.

Method	OPF	Default			Cluttered		
		AP_{50}	AP_{75}	$AP_{50:95}$	AP_{50}	AP_{75}	$AP_{50:95}$
SaG (Ours)	✓	98.7	96.6	87.8	88.6	81.0	73.0
SaG (Ours)		96.8	94.7	81.5	87.8	80.6	72.1
SaG no m_t	✓	98.3	95.9	81.6	86.1	78.2	69.1
SaG no h_t	✓	93.2	90.5	79.0	82.6	73.1	65.4
SaG grasp	✓	97.1	94.5	83.4	86.8	79.7	71.7
SaG push	✓	96.7	94.1	80.1	85.7	77.0	69.7
SaG push		94.2	92.0	77.7	85.5	76.9	68.2
SaG-maskone	✓	98.0	95.7	86.0	87.3	77.9	70.5
SaG-maskall	✓	97.9	95.7	86.0	85.6	77.1	69.5
VPG [43]	✓	89.2	86.3	69.4	81.4	72.1	65.0
SelfDeepMask [11]	✓	77.4	66.4	53.7	52.0	32.0	29.9
SelfDeepMask [11]		74.6	62.1	50.4	43.9	26.9	24.6
DeepMask [31]	✓	71.9	48.0	41.1	50.4	31.4	29.3
SBI [30]		72.1	54.2	45.6	52.8	29.1	27.3

5.3 Interactive Segmentation

We evaluate the instance segmentation performance for different baselines with Detectron2 [37] transfer learning in simulation. We fine-tune the Detectron2 COCO instance segmentation ResNet-50-FPN backbone for 200, 250 and 150 iterations for toy blocks 2000 interactions, YCB objects 2000 interactions and real robot unseen objects 1000 interactions. Our models are trained with initial learning rate of 0.0005 with SGD for optimization. Weight decay and momentum are set as 0.0001 and 0.9. All our models are trained on a single NVIDIA RTX 2080ti.

Given that the push proposal network in **SelfDeepMask** [11] and the complete data collection pipeline of **Seg-by-Interaction (SBI)** are not released,



Fig. 5. Basic toy blocks segmentation qualitative results. The top row is related to a default test case and the bottom row is the highly cluttered test case.

we prepare the training data with our SaG policy and only finetune their corresponding segmentation models. The baselines comparison in such a way can be slightly unfair since we didn’t use all entries from the previous works. However, we follow their default hyperparameter setting and the loss function selections and finetune the pretrained ResNet-50 *DeepMask* model 10 epochs. For **DeepMask** [31] method, we fine-tune the same model for 10 epochs.

Toy Blocks Segmentation The quantitative results are in Table 1. We use the standard COCO instance segmentation average precision (AP) for segmentation evaluation. In Table 1, *OPF* denotes the use of optical flow filtering classifier. Our proposed approach combining pushing and grasping interactions provides the optimal performance of mAP 87.8% in default setting and 73.0% in highly cluttered test setting. The **SaG push** method has relatively low performance since the singulation policy may move multiple objects simultaneously creating noisy labels. Our approach outperforms **SelfDeepMask** and by a large margin. Fig. 5 shows the visualization results.

Table 2. Segmentation results in simulation with YCB objects [5].

Method	<i>OPF</i>	Default			Cluttered		
		AP_{50}	AP_{75}	$AP_{50:95}$	AP_{50}	AP_{75}	$AP_{50:95}$
SaG (Ours)	✓	92.9	82.8	73.9	84.7	66.8	61.7
SaG (Ours)		91.7	82.7	73.1	81.5	65.1	58.7
SelfDeepMask [11]	✓	72.0	37.8	38.7	52.6	22.8	25.6
SelfDeepMask [11]		70.4	39.1	38.6	51.6	23.3	25.6
DeepMask [31]	✓	69.8	28.2	33.6	51.3	18.9	23.6
SBI [30]		68.3	26.5	32.2	47.7	14.9	20.8

YCB Objects Segmentation We also compare baselines with more complicated objects in high clutteredness scenarios. The quantitative results are in Table



Fig. 6. YCB objects segmentation qualitative results. The top row shows default test setting and bottom row is the cluttered test case.

2. Our method achieves 73.9% and 61.7% AP in default and cluttered test sets, respectively. Segmentation visualization can be found in Fig. 6.

5.4 SaG Downstream Robot Tasks Application

We evaluate the robotic top-down grasping task as one of the downstream tasks evaluated in simulation. The grasping performance is defined as % grasping success over the last 1000 attempts. We compare the grasping success rate with VPG [43] (no segmentation input at all), UOIS-VPG and SaG-VPG, where UOIS-VPG uses UOIS [39] as the segmentation model and SaG-VPG uses the fine-tuned Mask-RCNN to provide object binary masks information as an additional input. All three methods that execute only the grasping actions are trained from scratch for 1000 epochs with 6 toy blocks. The experiment results in Table 3 show that the SaG based segmentation model is able to improve the grasping performance.

Table 3. Top-down grasping success rate in simulation

Settings	SaG-VPG	UOIS-VPG	VPG
6 toy blocks	85.5	78.9	70.7
10 toy blocks	78.4	73.8	61.3

5.5 Real Robot Experiments

We collect the training data via our SaG pipeline with a Franka Emika Panda robot. The **SaG** policy is only trained in simulation but not fine-tuned in real-robot setting. There are 41 different objects in the training set and 25 novel objects in the default testing set as shown in Fig. 7.

Table 4. Segmentation results on real robot.

Method	OPF	Default			Cluttered		
		AP_{50}	AP_{75}	$AP_{50:95}$	AP_{50}	AP_{75}	$AP_{50:95}$
SaG (Ours)	✓	94.6	87.0	69.3	84.3	78.4	63.2
SaG (Ours)		88.1	80.0	61.1	85.3	78.3	62.5
SelfDeepMask [11]	✓	79.9	57.7	51.3	70.7	51.9	43.8
SelfDeepMask [11]		74.1	53.3	47.1	69.3	50.6	43.1
DeepMask [31]	✓	72.8	39.5	38.8	66.5	50.0	39.6

Table 5. SOTA comparison with the non-interactive approach on highly cluttered unseen object segmentation.

Method	Overlap			Boundary		
	P	R	F	P	R	F
SaG (Ours)	91.4	89.5	90.4	79.3	81.2	80.1
UOIS [39]	70.8	76.7	73.6	38.5	73.6	50.3

The quantitative segmentation results with different AP thresholds are in Table 4. Our approach outperforms (AP at 0.5) **SelfDeepMask** by 14.7 average precision points and **DeepMask** by 21.8 average precision points on default test cases, respectively. We also compare our method with pretrained UOIS [39] non-interactive approach in Table 5.

The qualitative visualizations are in Fig. 8 and Fig. 9. The results also show that our segmentation model can be generalized to novel objects. Even in a cluttered scene, our model manages to segment individual objects. Fig. 10 shows the interactive segmentation in a push experiment, where the singulation motion separates objects also contributes to the segmentation task.

6 Conclusions

This paper presents an interactive object segmentation method through an end-to-end SaG deep Q-learning approach. The robot interacts with unseen objects using pushing and grasping actions which automatically generate ground truth annotations for further finetuning. We show the segmentation results in both simulation and real-robot experiments outperforms several baselines by large margins. Additionally, the proposed approach can also be used in downstream robot manipulation tasks.

The limitation of our work suggests two possible directions for future work. Although effective, the current optical-flow based classifier lowers the data collection efficiency. The first direction is to learn a motion grouping method that directly provides multiple ground truth masks from optical flow. The other direction is to provide a singulation policy that moves one object at a time while improve the grasping success rate.

Acknowledgements: This work was supported in part by the Sony Research Award Program and NSF Award 2143730.



Fig. 7. Training and default testing object sets in real-robot experiments. The testing objects are never seen during training process.



Fig. 8. Highly cluttered test set visualization in real robot experiments.



Fig. 9. Visualizations of default test cases (sparsely distributed, a cluttered scene and multiple piles of objects).

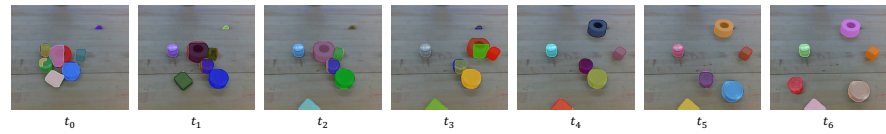


Fig. 10. Instance segmentation visualization with increasing number of pushes. Our singulation policy helps improve the segmentation results by breaking the clutter.

References

1. Badrinarayanan, V., Kendall, A., Cipolla, R.: Segnet: A deep convolutional encoder-decoder architecture for image segmentation. *IEEE transactions on pattern analysis and machine intelligence* **39**(12), 2481–2495 (2017) [18](#)
2. Boerdijk, W., Sundermeyer, M., Durner, M., Triebel, R.: Self-supervised object-in-gripper segmentation from robotic motions. *arXiv preprint arXiv:2002.04487* (2020) [3](#)
3. Bohg, J., Hausman, K., Sankaran, B., Brock, O., Kragic, D., Schaal, S., Sukhatme, G.S.: Interactive perception: Leveraging action in perception and perception in action. *IEEE Transactions on Robotics* **33**(6), 1273–1291 (2017) [3](#)
4. Byravan, A., Fox, D.: Se3-nets: Learning rigid body motion using deep neural networks. In: 2017 IEEE International Conference on Robotics and Automation (ICRA). pp. 173–180. IEEE (2017) [3](#)
5. Calli, B., Walsman, A., Singh, A., Srinivasa, S., Abbeel, P., Dollar, A.M.: Benchmarking in manipulation research: Using the yale-cmu-berkeley object and model set. *IEEE Robotics Automation Magazine* **22**(3), 36–52 (2015). <https://doi.org/10.1109/MRA.2015.2448951> [8](#), [11](#)
6. Chaudhary, K., Au, C.W., Chan, W.P., Nagahama, K., Yaguchi, H., Okada, K., Inaba, M.: Retrieving unknown objects using robot in-the-loop based interactive segmentation. In: 2016 IEEE/SICE International Symposium on System Integration (SII). pp. 75–80. IEEE (2016) [3](#)
7. Chen, Y., Ju, Z., Yang, C.: Combining reinforcement learning and rule-based method to manipulate objects in clutter. In: 2020 International Joint Conference on Neural Networks (IJCNN). pp. 1–6. IEEE (2020) [3](#)
8. Coleman, T.F., Moré, J.J.: Estimation of sparse Jacobian matrices and graph coloring problems. *SIAM journal on Numerical Analysis* **20**(1), 187–209 (1983) [6](#)
9. Dave, A., Tokmakov, P., Ramanan, D.: Towards segmenting anything that moves (2020) [9](#)
10. Deng, Y., Guo, X., Wei, Y., Lu, K., Fang, B., Guo, D., Liu, H., Sun, F.: Deep reinforcement learning for robotic pushing and picking in cluttered environment. In: 2019 IEEE/RSJ International Conference on Intelligent Robots and Systems (IROS). pp. 619–626. IEEE (2019) [3](#)
11. Eitel, A., Hauff, N., Burgard, W.: Self-supervised transfer learning for instance segmentation through physical interaction. In: 2019 IEEE/RSJ International Conference on Intelligent Robots and Systems (IROS). pp. 4020–4026. IEEE (2019) [2](#), [3](#), [7](#), [8](#), [10](#), [11](#), [13](#)
12. Eitel, A., Hauff, N., Burgard, W.: Learning to singulate objects using a push proposal network. In: *Robotics research*, pp. 405–419. Springer (2020) [2](#), [4](#)
13. Fang, K., Bai, Y., Hinterstoisser, S., Savarese, S., Kalakrishnan, M.: Multi-task domain adaptation for deep learning of instance grasping from simulation. In: 2018 IEEE International Conference on Robotics and Automation (ICRA). pp. 3516–3523. IEEE (2018) [1](#)
14. Fitzpatrick, P.: First contact: an active vision approach to segmentation. In: *Proceedings 2003 IEEE/RSJ International Conference on Intelligent Robots and Systems (IROS 2003)*(Cat. No. 03CH37453). vol. 3, pp. 2161–2166. IEEE (2003) [3](#)
15. He, K., Gkioxari, G., Dollár, P., Girshick, R.: Mask r-cnn. In: *Proceedings of the IEEE international conference on computer vision*. pp. 2961–2969 (2017) [8](#)
16. He, K., Zhang, X., Ren, S., Sun, J.: Deep residual learning for image recognition. In: *Proceedings of the IEEE conference on computer vision and pattern recognition*. pp. 770–778 (2016) [6](#)

17. Hermans, T., Rehg, J.M., Bobick, A.: Guided pushing for object singulation. In: 2012 IEEE/RSJ International Conference on Intelligent Robots and Systems. pp. 4783–4790. IEEE (2012) [4](#)
18. Huang, B., Han, S.D., Boularias, A., Yu, J.: Dipn: Deep interaction prediction network with application to clutter removal. arXiv preprint arXiv:2011.04692 (2020) [3](#)
19. Huang, G., Liu, Z., Van Der Maaten, L., Weinberger, K.Q.: Densely connected convolutional networks. In: Proceedings of the IEEE conference on computer vision and pattern recognition. pp. 4700–4708 (2017) [6](#)
20. Ilg, E., Mayer, N., Saikia, T., Keuper, M., Dosovitskiy, A., Brox, T.: Flownet 2.0: Evolution of optical flow estimation with deep networks. In: Proceedings of the IEEE conference on computer vision and pattern recognition. pp. 2462–2470 (2017) [8](#)
21. Ioffe, S., Szegedy, C.: Batch normalization: Accelerating deep network training by reducing internal covariate shift (2015) [19](#)
22. Kenney, J., Buckley, T., Brock, O.: Interactive segmentation for manipulation in unstructured environments. In: 2009 IEEE International Conference on Robotics and Automation. pp. 1377–1382. IEEE (2009) [3](#)
23. Kiatos, M., Malassiotis, S.: Robust object grasping in clutter via singulation. In: 2019 International Conference on Robotics and Automation (ICRA). pp. 1596–1600. IEEE (2019) [4](#)
24. Kurenkov, A., Taglic, J., Kulkarni, R., Dominguez-Kuhne, M., Garg, A., Martín-Martín, R., Savarese, S.: Visuomotor mechanical search: Learning to retrieve target objects in clutter. In: 2020 IEEE/RSJ International Conference on Intelligent Robots and Systems (IROS). pp. 8408–8414. IEEE (2020) [1](#)
25. Kuzmič, E.S., Ude, A.: Object segmentation and learning through feature grouping and manipulation. In: 2010 10th IEEE-RAS International Conference on Humanoid Robots. pp. 371–378. IEEE (2010) [3](#)
26. Le Goff, L.K., Mukhtar, G., Le Fur, P.H., Doncieux, S.: Segmenting objects through an autonomous agnostic exploration conducted by a robot. In: 2017 First IEEE International Conference on Robotic Computing (IRC). pp. 284–291. IEEE (2017) [3](#)
27. Liang, H., Lou, X., Yang, Y., Choi, C.: Learning visual affordances with target-orientated deep q-network to grasp objects by harnessing environmental fixtures. In: 2021 IEEE International Conference on Robotics and Automation (ICRA). pp. 2562–2568. IEEE (2021) [1](#)
28. Lin, T.Y., Maire, M., Belongie, S., Hays, J., Perona, P., Ramanan, D., Dollár, P., Zitnick, C.L.: Microsoft coco: Common objects in context. In: European conference on computer vision. pp. 740–755. Springer (2014) [2](#)
29. Nair, V., Hinton, G.E.: Rectified linear units improve restricted boltzmann machines. In: Icml (2010) [19](#)
30. Pathak, D., Shentu, Y., Chen, D., Agrawal, P., Darrell, T., Levine, S., Malik, J.: Learning instance segmentation by interaction. In: Proceedings of the IEEE Conference on Computer Vision and Pattern Recognition Workshops. pp. 2042–2045 (2018) [2](#), [3](#), [10](#), [11](#)
31. Pinheiro, P.O., Collobert, R., Dollár, P.: Learning to segment object candidates. arXiv preprint arXiv:1506.06204 (2015) [10](#), [11](#), [13](#)
32. Rohmer, E., Singh, S.P., Freese, M.: V-rep: A versatile and scalable robot simulation framework. In: 2013 IEEE/RSJ International Conference on Intelligent Robots and Systems. pp. 1321–1326. IEEE (2013) [9](#)

33. Russakovsky, O., Deng, J., Su, H., Krause, J., Satheesh, S., Ma, S., Huang, Z., Karpathy, A., Khosla, A., Bernstein, M., et al.: Imagenet large scale visual recognition challenge. *International journal of computer vision* **115**(3), 211–252 (2015) [2](#), [8](#)
34. Sarantopoulos, I., Kiatos, M., Doulgeri, Z., Malassiotis, S.: Split deep q-learning for robust object singulation. In: 2020 IEEE International Conference on Robotics and Automation (ICRA). pp. 6225–6231. IEEE (2020) [4](#)
35. Schiebener, D., Ude, A., Asfour, T.: Physical interaction for segmentation of unknown textured and non-textured rigid objects. In: 2014 IEEE International Conference on Robotics and Automation (ICRA). pp. 4959–4966. IEEE (2014) [3](#)
36. Spelke, E.S.: Principles of object perception. *Cognitive science* **14**(1), 29–56 (1990) [2](#)
37. Wu, Y., Kirillov, A., Massa, F., Lo, W.Y., Girshick, R.: Detectron2. <https://github.com/facebookresearch/detectron2> (2019) [8](#), [10](#)
38. Xie, C., Xiang, Y., Mousavian, A., Fox, D.: The best of both modes: Separately leveraging rgb and depth for unseen object instance segmentation. In: Conference on robot learning. pp. 1369–1378. PMLR (2020) [1](#)
39. Xie, C., Xiang, Y., Mousavian, A., Fox, D.: Unseen object instance segmentation for robotic environments. *IEEE Transactions on Robotics* pp. 1–17 (2021) [1](#), [5](#), [12](#), [13](#)
40. Xu, K., Yu, H., Lai, Q., Wang, Y., Xiong, R.: Efficient learning of goal-oriented push-grasping synergy in clutter. arXiv preprint arXiv:2103.05405 (2021) [1](#), [6](#)
41. Yang, Y., Liang, H., Choi, C.: A deep learning approach to grasping the invisible. *IEEE Robotics and Automation Letters* **5**(2), 2232–2239 (2020) [3](#), [4](#), [6](#), [8](#)
42. Zeng, A., Song, S., Lee, J., Rodriguez, A., Funkhouser, T.: Tossingbot: Learning to throw arbitrary objects with residual physics. *IEEE Transactions on Robotics* **36**(4), 1307–1319 (2020) [18](#)
43. Zeng, A., Song, S., Welker, S., Lee, J., Rodriguez, A., Funkhouser, T.: Learning synergies between pushing and grasping with self-supervised deep reinforcement learning. In: 2018 IEEE/RSJ International Conference on Intelligent Robots and Systems (IROS). pp. 4238–4245. IEEE (2018) [3](#), [4](#), [6](#), [7](#), [9](#), [10](#), [12](#), [18](#)

A More Method Details

A.1 SaG Policy Algorithm

Our interaction policy can be summarized as follows:

Algorithm 1 Interaction Policy

Input: RGB-D image I , density threshold p ;

Output: action decision a_t at time t ;

```

1:  $H, M \leftarrow \text{ObjectSegmentation}(I)$ ;
2: if  $\text{density}(H) > p$  then
3:    $s_t \leftarrow \text{HeightmapProjection}(I, H, M)$ 
4:    $Q_p \leftarrow \Phi_p(s_t)$ 
5:    $a_t \leftarrow \arg \max_a Q_p$ 
6: else
7:    $M \leftarrow \text{AllOnesMask}()$ 
8:    $s_t \leftarrow \text{HeightmapProjection}(I, H, M)$ 
9:    $Q_g \leftarrow \Phi_g(s_t)$ 
10:   $a_t \leftarrow \arg \max_a Q_g$ 
11: end if

```

A.2 Implementation and Training Details

The deep Q-learning network in our work is an encoder-decoder fully convolutional network [1]. Both push net ϕ_p and grasp net ϕ_g have a structure of a 3-layer residual network followed by bilinear upsampling.

The training objective is to minimize the temporal difference error δ_t

$$\delta_t = Q_\pi(\theta_t; s_t, a_t) - (R_{a_t}(s_t, s_{t+1}) + \gamma \max_a Q_\pi(\theta_t^-; s_{t+1}, a)) \quad (4)$$

using the Huber loss function [42]

$$\mathcal{L}_\delta = \begin{cases} \frac{1}{2} \delta_t^2, & \text{if } |\delta_t| \leq 1 \\ |\delta_t| - \frac{1}{2}, & \text{otherwise} \end{cases} \quad (5)$$

where θ_t are the DQN parameters at time t , and the target network parameters θ_t^- are held fixed between updates. Only the single-pixel gradient where the motion primitive is executed in each iteration was computed and allowed to pass through the DQN. All other pixels backpropagate with 0 loss as in [43].

Multi-stage training is used. In the first two stages, the cluttered scenario is formulated with six objects in singulation training. Eight objects are randomly dropped in the workspace for grasping training. We train the singulation policy for 2500 episodes and the grasping policy for 1500 episodes, respectively. The

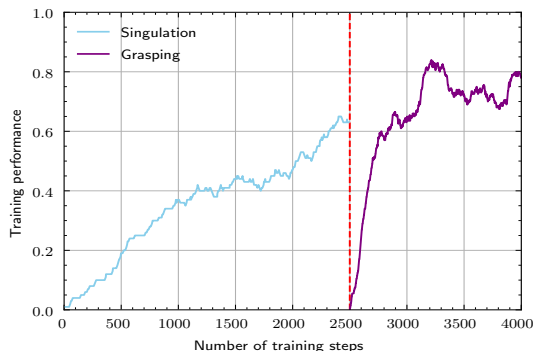


Fig. 11. Training performance. The blue line demonstrates that the singulation success rate reaches over 60% in 2500 iterations, while the grasping performance achieves about 80% in 1500 iterations.

coordination stage finally matches the data distribution of the two policies and is trained for 1500 episodes.

The training curve is shown in Fig. 11. In stage one, we calculate the c^i center location pairwise distance after each interaction and form a graph. When the graph density reaches zero in one trial, we define it as a successful trial. The singulation performance is defined as % singulation success over the last 100 trials. When the number of pushing action reaches a maximum number of 10, we claim it as a failed trial. The grasping performance is defined as % grasping success over the last $j = 200$ attempts.

The optical flow binary classifier takes as inputs the FlowNet2 generated optical flow and task relevant features. The optical flow is fed into a pretrained ResNet-101 encoder and task features are passed into a simple MLP (three fully connected layers with batch normalization [21] and RELU [29]). We concatenate the two outputs and finally pass to a fully connect layer to output a single dimension probability. We use the binary cross-entropy loss to train the classifier.

A.3 More Visualizations

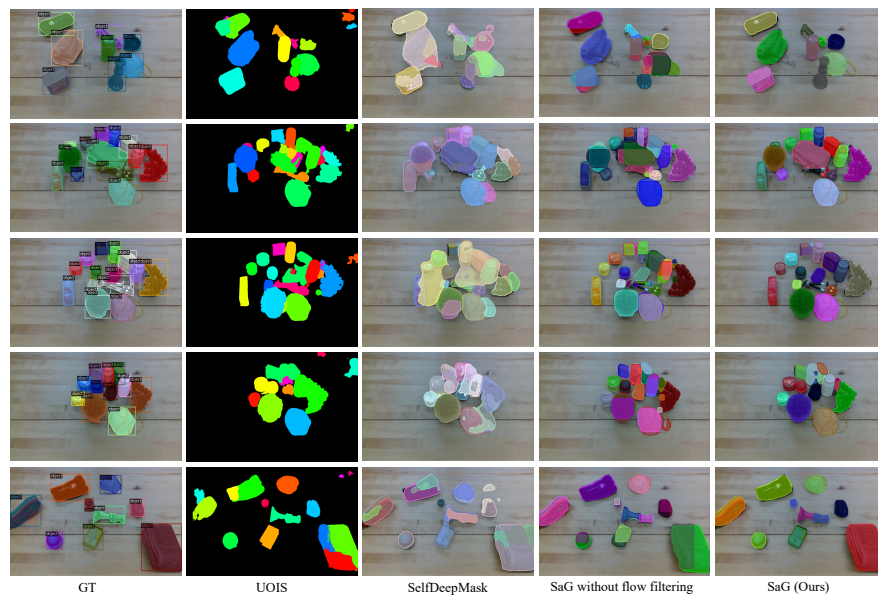


Fig. 12. More visualizations of real robot test cases.